The International Multi-Tokamak Profile Database

The ITER 1D Modelling Working Group: D. Boucher[a], J.W. Connor[b], W.A. Houlberg[c], M.F. Turner[b], G. Bracco[d], A. Chudnovskiy[a,e], J.G. Cordey[b], M.J. Greenwald[f], G.T. Hoang[g], G.M.D. Hogeweij[h], S.M. Kaye[i], J.E. Kinsey[j], D.R. Mikkelsen[i], J. Ongena[k], D.R. Schissel[l], H. Shirai[m], J. Stober[n], P.M. Stubberfield[b], R.E. Waltz[l], J. Weiland[o]

[a] ITER Naka Joint Work Site, Naka, Ibaraki, Japan
[b] Euratom/UKAEA Fusion Association, Culham Science Centre, Abingdon, Oxfordshire, UK
[c] Oak Ridge National Laboratory, Oak Ridge, Tennessee, USA
[d] Associazione Euratom–ENEA sulla Fusion, CRE Frascati, Rome, Italy
[e] Russian Research Center, Kurchatov Institute, Moscow, Russian Federation
[f] Massachusetts Institute of Technology, Cambridge, Massachusetts, USA
[g] Association Euratom–CEA, Centre d'études de Cadarache, France
[h] FOM Institute for Plasma Physics, Rijnhuizen, Nieuwegein, Netherlands
[i] Princeton Plasma Physics Laboratory, Princeton University, Princeton, New Jersey, USA
[j] Lehigh University, Bethlehem, Pennsylvania, USA
[k] Ecole Royale Militaire/Köninglijke Militaire School, Association Euratom–Belgian State, Brussels, Belgium
[l] General Atomics, San Diego, California, USA
[m] Japan Atomic Energy Research Institute, Naka, Ibaraki, Japan
[n] Max-Planck-Institut für Plasmaphysik, Euratom Association Garching, Germany
[o] Chalmers University of Technology, Goteborg, Sweden

Abstract. An international multi-tokamak profile database has been assembled, constituting a representative set of reference tokamak discharges for the purpose of testing local transport models against well documented data. In particular, it will allow one to measure the accuracy with which the models can reproduce experiments and draw confidence intervals for the predictions of the models outside the range covered in the database. This database is now available to the fusion community and may be accessed by anonymous ftp to iterphys.naka.go.jp; the purpose of this article is to describe the structure of the database and the discharges contributing to it so that all can take full advantage of this resource. Thus, after an introductory general discussion of the database, there is a more detailed description of its structure, with listings of variables emphasized and how to access the database. There is then a brief description of each contributing tokamak and information on the type of discharges available from that tokamak. This is followed by a more quantitative description of the data, giving the ranges of dimensional and dimensionless variables available. Some typical modelling results to illustrate the use of the database are given in the conclusion.

1. Introduction

Predictions of the performance of next step devices are often based on the use of empirical scaling laws. In order to establish these, multimachine databases have been established under the auspices of the ITER Engineering Design Activities: the L mode [1] and H mode [2] energy confinement time databases and the H mode power threshold database [3]. However, it would be desirable to develop and validate 1-D transport models to make confinement predictions; these would be more powerful, being able to predict profiles of temperature and density for the various particle species present in a tokamak, and, preferably, would have a physics basis underlying them. A number of theoretical models for the anomalous heat and particle transport in tokamaks have been developed by the fusion community over the years. Some of these are physics based, such as the ion temperature gradient (ITG) turbulent transport models of Kotschenreuther et al. [4] and Waltz et al. [5], the drift wave transport multimode model of Kinsey and Bateman [6] and the current diffusive ballooning model of Itoh et al. [7]; others are

semi-empirical, involving some theoretically based ingredients together with empirical elements, such as the Rebut–Lallia–Watkins model [8], the mixed shear model of Taroni and co-workers [9] or the canonical profiles transport model of Dnestrovskij et al. [10]. Previously, tests of these models have been partial, restricted to particular discharges from particular tokamaks and different discharges for each model; furthermore no standardized methodology of testing existed. Consequently, transport modelling results were treated with some scepticism, even if this was undeserved.

To remedy this situation the International (formerly ITER) Profile Database has been developed [11]. A version of this database was made available to the fusion community in late 1998. This first public release can be accessed by means of a database server, currently located at the ITER Joint Central Team, Naka, Japan. In this article we describe this 1998 public release version. However, new discharges are regularly being processed for placing on the database and subsequent public releases can be expected to contain these additional discharges. The objective of the profile database is to provide, in one easily accessible form, all the information transport modellers would need to include in their transport codes to simulate a particular tokamak discharge and to compare the output of the predictions against the measured data. Thus, for each tokamak discharge listed the database normally contains

(a) A general description with comments to characterize its principal features, e.g. the form of heating and the confinement mode;
(b) A list of global quantities which remain constant through the discharge, such as toroidal field, and others, such as plasma composition or neutral beam energy, at a selected time point during the discharge;
(c) Time traces for quantities such as plasma current, line averaged density or heating power;
(d) Profiles of quantities such as electron and ion temperatures and densities, the safety factor and heat and particle deposition at specified times (or as a function of time, if possible).

The profiles are given as functions of the square root of the normalized toroidal flux, ρ. Geometrical quantities, such as the flux surface averaged objects $\langle|\nabla\rho|^2\rangle$ needed for solving 1-D transport equations, are also provided. The structure of the database, how it is accessed and the definitions of variables are given in more detail in Section 2, with additional information in Appendices A–F (a full database manual is available on-line by accessing the database server); Section 2 also presents a standard form of the 1-D power and particle balance equations to be used for model testing.

This multimachine database comprises a representative set of reference discharges drawn from the majority of the world's tokamaks. It continues to develop, but currently contains data from ASDEX Upgrade, Alcator C-Mod, DIII-D, FTU, JET, JT-60U, RTP, T-10, TFTR, Tore Supra and TEXTOR. The discharges entered in the database contain: a wide range of confinement modes, e.g. ohmic, L mode, H mode (with a variety of ELM types), supershots, optimized shear modes (including negative central shear and enhanced reverse shear with ITBs), radiative impurity modes, hot ion and hot electron modes; a range of isotopes, including DT shots; transient situations, e.g. impurity injection and cold pulse experiments; and a number of additional heating methods, e.g. NBI, ICRH, ECRH and lower hybrid (LH) wave heating. The discharges from each machine are submitted by a 'data provider' associated with that machine. Summaries of the general characteristics of each contributing tokamak and the nature of the discharges provided, together with references, are presented in Section 3.

In order to carry out systematic studies of the performance of transport models, it is important to be able to carry out scans over a number of variables, both dimensional (e.g. $\overline{n}$, B_T, I_p, P, R, a, ...) and dimensionless (e.g. ρ_*, ν_*, β, n/n_{GW}, M, q, ε ...) ones. Here $\bar{n}$ is the line averaged density, B_T the toroidal magnetic field, I_p the plasma current, P the auxiliary heating power, R the major radius and a the minor radius, while ρ_* is the normalized ion Larmor radius, ν_* the collisionality parameter, β the ratio of plasma and magnetic energy, n_{GW} the Greenwald density, M the toroidal Mach number, V_T/c_s, where V_T is the toroidal plasma velocity and c_s the sound speed, q the safety factor and ε the inverse aspect ratio. One is also interested in variation with respect to shaping parameters (e.g. κ, the plasma elongation) and plasma compositional parameters (e.g. A_i, T_e/T_i, Z_{eff}, where A_i is the atomic mass number, T_e and T_i are characteristic electron and ion temperatures, and Z_{eff} is effective charge). Section 4 provides a detailed and quantitative description of the data available in terms of these parameters. There are also plots showing the parameter space for various dimensional and

dimensionless global variables, as well as some 'local' profile ones evaluated at $\rho = 0.5$, e.g. R/L_T, R/L_n and η_i. Here L_T and L_n are temperature and density gradient lengths, respectively, and η_i is the ratio of L_n to L_{Ti}.

Ways in which the database has been used for the testing of transport models have been presented previously in Refs [11–13] and an illustrative example is given here in Section 5. Although the database was developed in order to test transport models it also has the potential to be of value for other uses requiring profile data, e.g. comparing theoretical models for MHD stability criteria with the onset of events such as sawteeth and tearing modes. Finally, a summary and discussion of the article appears in Section 6.

Table 1. Machine directories

Directory name	Tokamak machine
aug	ASDEX Upgrade
cmod	Alcator C-Mod
d3d	DIII-D
ftu	FTU
jet	JET
jt60u	JT-60U
rtp	RTP
t10	T-10
tftr	TFTR
ts	Tore Supra
txtr	TEXTOR

2. Description of database structure

2.1. General

2.1.1. Database access

The International Profile Database (formerly known as the ITER Profile Database) is stored on a server at the ITER Joint Working Site at Naka, Japan, and may be accessed by anonymous ftp to iterphys.naka.jaeri.go.jp. The data files and other information relating to the 1998 release of the database can then be found in the pub/ITERProfileDatabase1998 directory. Directories containing subsequent releases of the database will be named for the relevant year. Within the main (pub/ITERProfileDatabase1998) directory is contained a file named 'NOTICE'. This file contains advice on use of the material in the database and users are requested to download this file and read the information therein before proceeding any further.

2.1.2. Database structure

The International Profile Database could more accurately be called a file store. The information pertaining to each discharge is contained within a set of files (usually four files) grouped together in a subdirectory named by the discharge number. These discharge subdirectories are grouped into higher level directories according to the tokamak machine from which they derive. The machine directories are then situated within the main directory. These machine directories are listed in Table 1.

A number of other directories exist alongside the machine directories and these contain supplementary material which may assist the database user to locate and interpret the information within the discharge data files. This supplementary material is described in more detail in Section 2.4.

2.1.3. Data files

Normally three main data files are provided for each discharge. These are:

(a) A '0-D' file containing values for a given set of global variables at one or more fixed time points.
(b) A '1-D' file containing time traces of a number of global variables.
(c) A '2-D' file containing profiles of local plasma quantities, e.g. density and temperature.

The content and arrangement of the data within these files is discussed in more detail in Sections 2.2 and 2.3. Each file is named according to a strict convention and is of the form

PR*yy*_*tok*#####_*n*d.dat

where
yy denotes the year of release
tok is the machine directory name
is the discharge number (usually five or more digits)
$n = 0, 1$ or 2 according to file type (0-D, 1-D or 2-D).

Thus the tree name for each file, within the main directory for the 1998 release, is given by:

tok/#####/PR98_*tok*_#####_*n*d.dat

e.g.

tftr/45950/PR98_tftr_45950_1d.dat

It is normally expected that all three files should exist for each discharge. However in a few cases the 1-D file is absent, although this may be compensated for by the presence of global data at more than one time point in the 0-D file. For some discharges an extra data file is provided which contains further useful experimental data.

2.1.4. Comment files

A fourth file may also exist alongside the main data files. This is designated by the name

PR*yy_tok_*#####_com.dat

and contains general useful information concerning the particular discharge.

2.2. Content of the data files

2.2.1. 0-D File: global variables

The 0-D files contain the values of 78 global variables at one or more specified time points. The names of these variables are listed in Appendix A with summaries of their definitions. Further information can be found in the reference manual (Section 2.4). The selected time points are expected to typify specific regimes in the discharge. While this file can be useful for some purposes, one must exercise some caution, since values of some of the variables may be hand entered and therefore they may not always be given to a fine degree of accuracy and occasionally the format does not comply with the standard. Furthermore, different tokamaks use different definitions for shape parameters such as κ and δ. Where there is a discrepancy between the 1-D or 2-D data and the 0-D data, the 1-D or 2-D data should be used in preference.

2.2.2. 1-D File: time traces of global variables

The 1-D files contain time traces of certain variables over a time range of significance for the discharge. The set of 16 variables for which time traces are expected to exist is listed in Appendix B, along with summary definitions. Time traces of another 14 variables (e.g. the loop voltage, internal plasma inductance, q_{95}, total and thermal energy contents, and central ion and electron temperatures) may also exist for some discharges. Further information and full definitions can be found in the reference manual (Section 2.4).

2.2.3. 2-D File: local transport quantities

The 2-D files contain radial profiles of certain global variables at one or more time points of significance for the discharge. Normally profiles will exist at least for the time point or points specified in the 0-D file; however for many discharges, profiles are provided at reasonably close intervals for the complete time range of the traces in the 1-D file, enabling the construction of a 3-D picture of the time evolution of many plasma parameters. The radial co-ordinate for these profiles is the square root of the normalized toroidal flux ρ, defined as follows:

$$\rho = \sqrt{\frac{\phi}{\phi_a}} \tag{1}$$

where ϕ is the total toroidal flux enclosed by the given magnetic surface, ϕ_a is the total toroidal flux enclosed by the plasma separatrix or limiter (database 1-D variable number 29 (PHIA)) and ρ varies from 0 in the centre to 1 at the separatrix/limiter.

The following form is assumed for the particle and energy conservation equations:

$$\frac{\partial}{\partial t} n_\alpha + \frac{1}{V'} \frac{\partial}{\partial \rho} V' \langle |\boldsymbol{\nabla}\rho| \rangle \tilde{\Gamma}_\alpha = S_\alpha \tag{2}$$

$$\frac{\partial}{\partial t} W_\alpha + \frac{1}{V'} \frac{\partial}{\partial \rho} V' \left(-n_\alpha \chi_\alpha \langle |\boldsymbol{\nabla}\rho|^2 \rangle \frac{\partial}{\partial \rho} T_\alpha + \langle |\boldsymbol{\nabla}\rho| \rangle \frac{3}{2} \tilde{\Gamma}_\alpha T_\alpha \right) = \mathrm{CMP} + Q_\alpha \tag{3}$$

where α stands for either thermal electrons (e) or main thermal ions (i).

The compressional term, CMP, is theory dependent and needs to be specified for each model; e.g. for Braginskii collisional transport,

$$\mathrm{CMP} = -n_\alpha k T_\alpha \langle \boldsymbol{\nabla} \cdot \boldsymbol{v}_\alpha \rangle \tag{4}$$

where $n_\alpha v_\alpha = \tilde{\Gamma}_\alpha$.

Symbols are defined in Table 2, where the numbers in the third column indicate which database variable(s), Appendix C, equate or contribute to that term in the equations.

The most commonly provided database variables are listed in Appendix C, with a cross-reference to the relevant terms of the above equations. The complete list of 2-D variables and their definitions can be found in the reference manual.

Table 2. Definitions of the symbols in the transport equations

Symbol	Definition	Relevant database 2-D variable numbers
T_α	Electron/ion temperature (eV)	1, 5
n_α	Electron/ion density (m^{-3})	9, 29, 38, 42, 42b, 46
Q_α	Power density (W m^{-3})	13–22, 50, 51, 62–65
S_α	Particle source (m^{-3} s^{-1})	23, 24, 61
$\frac{\partial}{\partial t}W_\alpha$	Rate of change of energy density (W m^{-3})	58, 59
$\frac{\partial}{\partial t}n_\alpha$	Rate of change of electron/ion density (m^{-3} s^{-1})	60
$\langle\lvert\nabla\rho\rvert\rangle$	Geometric term (m^{-1})	74
$\langle\lvert\nabla\rho\rvert^2\rangle$	Geometric term (m^{-2})	75
V	Volume enclosed by the magnetic surface (m^3); V' denotes a derivative of V with respect to ρ	69
χ_α	Estimated thermal electron/ion heat diffusivity (m^2 s^{-1})	36, 37
$\tilde{\Gamma}_\alpha$	Particle flux (m^{-2} s^{-1})	(not applicable)

2.3. Data file format

2.3.1. 0-D File

The format for the 0-D file follows the file format adopted for the 0-D H mode global database [2]. Thus the values of the 78 0-D variables for each discharge time slice are contained within 12 'records' each of 80 bytes in length. The variable values occupy adjacent fields, each of 11 bytes in length, within the record, where the final byte in each field is always left blank to act as a field separator. Hence the first 11 records each contain values of 7 variables with the final record containing just the value of the 78th variable.

The layout is presented in Appendix D, where the 12 rows represent the 12 database 'records' and the column headings show the initial byte for each separate field within the record. The table then gives the content and format of each field.

Where no value is supplied for a particular 0-D value the relative field is not left blank but is occupied by representational characters as follows:

(a) Missing character string: ????????
(b) Missing integer: -9999999
(c) Missing real: -9.999E-09

Software for reading 0-D files and turning the information into a user friendly table is provided on the server in the software subdirectory (Section 2.4.1). The complete set of 0-D data for all of the discharges in the database is concatenated into the file named 'PR98tokamak_0d.dat' within the main directory.

2.3.2. 1-D File

The 1-D description files are themselves composed of a list of files, one for each of the variables presented. The format for the variable files is ASCII Ufile as developed at Princeton Plasma Physics Laboratory by D. McCune. The first vector given is the time vector (the independent variable), followed by the data vector (containing the dependent variable).

The header for each separate file contains records of the following schematic form:

```
TIME    ;-INDEPENDENT VARIABLE LABEL: X-
IP      ;-DEPENDENT VARIABLE LABEL-
```

The field '-DEPENDENT VARIABLE LABEL-' contains the name of the variable as given in Appendix B or in the extended list in the reference manual.

Ufiles are separated by two lines of at least 10 '*' (ASCII code 42). An example of a single 1-D Ufile is presented in Appendix E.

Software information for reading Ufiles and various software for extracting and retrieving the data are provided in: /pub/profile_data/software (Section 2.4.1).

2.3.3. 2-D File

The 2-D file has the same format as the 1-D file except that the time vector is preceded by the radial vector ρ (the first independent variable). So the header for each separate file will contain records of the following schematic format:

Table 3. Main parameters of the discharges from the contributing tokamaks

Tokamak	R (m)	a (m)	B_T (T)	I_p (MA)	κ	P (MW)
ASDEX Upgrade	1.65	0.5	2.2–2.5	1.0	<1.8	5.1–7.7
Alcator C-Mod	0.68	0.22	5.3	0.8–1.0	1.6–1.75	1.0–2.6
DIII-D	1.7	0.65	1.0–2.25	0.5–2.0	<2.5	<15
FTU	0.93	0.3	5.3	0.5*	1	0.35
JET	<3.0	<1.1	1–3.1	1–3.2	1.4–1.72	<21
JT-60U	3.19–3.33	0.80–0.96	2.41–4.21	1.0–3.51	1.41–1.65	5.29–21.13
RTP	0.72	0.16	2.0–2.3	0.08	1	0.35
T-10	1.5	0.22–0.32	2.8–3.1	0.15–0.43	1	<2
TFTR	2.4	0.8	2.1–5.5	0.75–2.15	1	<35
Tore Supra	2.4	0.8	2.1–3.7	0.4–1.5	1	2.9–9.3
TEXTOR	1.75	0.46	2.25	0.4	1	2.86

* The FTU discharge is a current ramp-up: 0.3–0.5 MA.

```
RHO        ;-INDEPENDENT VARIABLE LABEL: X-
TIME       ;-INDEPENDENT VARIABLE LABEL: Y-
TE         ;-DEPENDENT VARIABLE LABEL-
```

In this case the field '-DEPENDENT VARIABLE LABEL-' contains the name of the variable as given in Appendix C or in the extended list in the reference manual.

An example of a single 2-D Ufile is presented in Appendix F. Here the first seven lines of data contain the 41 points of the ρ vector; the next line contains the two points of the time vector; and the remaining 14 lines contain the 82 points of the two data vectors. The file format dictates that the time vector and the first data vector should begin on new lines but all the data vectors are then written continuously.

2.4. Supplementary database material

2.4.1. Useful software

The subdirectory 'software/server_to_users' contains some software that users may find helpful for reading and interpreting Ufiles. The file 'ufile_read.tar' contains some simple stand-alone FORTRAN routines to read 1-D or 2-D ASCII Ufiles. Some words of explanation can be found in 'ufile_read.com'. The file 'Ufile_format' contains some discussion on the possible difficulties with consistency of data format between Ufiles from different sources.

The subdirectory 'software/ornl' contains further useful software, explanations of which can be found in the files 'README.stan' and 'ldread.txt'.

2.4.2. Datafile list

A list of all the data files contained within the database can be found in the file 'description.txt', located in the main directory. The file names are grouped under the machine name and discharge number, with a one line description of the discharge.

2.4.3. Reference manual

Full definitions of all parameters and variables used in the database are supplied in the reference manual which can be found in the 'documents' subdirectory as Manual_may_98.msw (for the MS word version) or Manual_may_98.ps (for the Postscript version).

3. Summary information on each machine

In this section we provide a brief summary of the characteristics of each tokamak contributing to the profile database, together with a description of the types of discharge submitted to the database. The main parameters of these tokamaks are shown in Table 3. It is also interesting to note (Table 4) the number of discharges and time slices provided in each tokamak.

3.1. ASDEX Upgrade

ASDEX Upgrade is a divertor tokamak with a major radius $R = 1.65$ m and a minor radius $a = 0.5$ m, a toroidal magnetic field $B_T = 1.3 - 3$ T and a plasma current $I_p = 0.4 - 1.4$ MA, with elongation κ

Table 4. The number of discharges and time slices provided by each tokamak

Tokamak	Number of discharges	Number of 0-D time slices
ASDEX Upgrade	2	3
Alcator C-Mod	5	5
DIII-D	27	33
FTU	1	1
JET	20	24
JT-60U	9	38
RTP	2	2
T-10	20	40
TFTR	107	111
Tore Supra	7	8
TEXTOR	1	1

<1.8, designed especially to study heat exhaust and particle control for a next step device and the development of appropriate divertor geometries. Therefore it is equipped with a high heating capability of 20 MW NBI, 6 MW ICRH and 2 MW ECRH. Open and closed divertor configurations have been analysed, including tungsten coated divertor plates. Other key issues of research are H mode physics, radiative mantle scenarios, MHD stability and active control and physics of ITBs in advanced tokamak scenarios. This will be the main emphasis in the future and increased current drive capabilities are at present installed for steady state operation of non-inductive scenarios as well as for current profile shaping in improved H mode scenarios. The two discharges submitted to the database are from the divertor I phase. One (discharge 6905) is in H mode with two time points with different heating powers. The other (discharge 6136) is a time point from a typical completely detached H mode (CDH) discharge, i.e. with a radiative mantle due to feedback controlled puffing of impurities [14]. Divertor II results, including steady state advanced scenarios and discharges which are dimensionlessly identical to corresponding JET discharges, are to be included in the database in the near future.

3.2. Alcator C-Mod

Alcator C-Mod is a compact high field tokamak with a closed divertor and capabilities for strong plasma shaping. It has major radius $R = 0.68$ m and minor radius $a = 0.22$ m, while its toroidal magnetic field and current lie in the ranges $2.6 < B_T$ (T) < 8.0 and $0.4 < I_p$ (MA) < 1.5 [15]. The standard equilibrium configuration is a single null divertor with plasma elongation in the range $\kappa = 1.6-1.75$. The plasmas are somewhat D shaped, with lower triangularity δ typically in the range 0.5−0.6 and upper triangularity typically in the range 0.3−0.4. The plasma line averaged density $\bar{n}_e$ ranged from 1.3×10^{20} to 4.3×10^{20} m^{-3} with better quality H modes, all above 2×10^{20} m^{-3}. The auxiliary heating method is ICRH, employing hydrogen minority in deuterium plasmas at $B_T = 5.3$ T as the principal scenario. For these experiments, up to 3.5 MW of RF power were available. Because of the large B/R ratio in Alcator C-Mod, ohmic heating is never negligible, contributing 0.5–1.5 MW depending on plasma temperature and purity. At the high densities that prevail, particularly in H mode, the plasma is essentially thermal with very little contribution to the stored energy from energetic ions (typically no more than 5%) and with $T_i \cong T_e$. Data in the profile database is for $B_T \cong 5.3$ T and I_p from 0.8 to 1.2 MA. Discharges in the database include ohmic, L mode, ELM-free and ELMy/EDA (enhanced D_α) H modes [16, 17]. Although no beams are used to directly impart momentum to the plasmas, the H mode discharges are observed to rotate strongly in the co-current direction with Mach numbers M in the range 0.2–0.3 [18].

3.3. DIII-D

DIII-D is a flexible tokamak capable of controlling the plasma geometry and the shapes of profiles [19]. It has a major radius $R = 1.7$ m, a minor radius $a = 0.65$ m and, typically, a toroidal field $B_T = 2.1$ T, a plasma current $I_p = 1.6$ MA and a nominal elongation of 1.65. It is equipped with a comprehensive set of diagnostic instruments, a 20 MW NBI heating system, an RF heating and current drive system, a pellet injector system for plasma fuelling and a pumped divertor system.

Data from 26 DIII-D discharges have been contributed to the profile database. Five pairs of L mode discharges in the database are scans in gyroradius where the normalized collisionality, plasma beta and safety factor were held constant. Discharges 69627, 69648, 78283, 78109, 71378 and 71384 [20–23] were neutral beam heated while discharges 78281, 78106, 78328 and 78316 were RF heated. In general, analysis of the data indicates that the electron thermal diffusivity followed a gyro-Bohm scaling while the ion thermal diffusivity followed a Goldston-like scaling. Scaling of the energy confinement time

varied from gyro-Bohm-like depending upon whether electrons or ions dominated the radial heat transport. The gyro-radius scaling results were independent of the method of auxiliary heating. Discharges 82205 and 82788 are a first attempt at an H mode gyro-radius scan on DIII-D [24]. These H mode discharges have the same plasma shape as well as the same beta, collisionality and safety factor as the ITER outline design. For these dimensionally similar discharges, both the electron and ion diffusivities scaled as gyro-Bohm-like, as did the global thermal confinement time. The other set of dimensionally similar discharges comprise scans in plasma beta in both L mode (Nos 90118 and 90105) and H mode (Nos 90117 and 90108) while holding the normalized gyroradius, collisionality and safety factor fixed [25]. Here, it was found that the normalized thermal confinement time $B\tau_{th}$ was nearly independent of beta with a slight favourable beta scaling found in the H mode pair.

In addition to scans in gyroradius and plasma beta, there are H mode scans in electron density, heating power and elongation in the database. Discharges 81321 and 81329 represent a 1.0 MA, 2.0 T H mode density scan at constant temperature [26, 27]. Power balance analysis of these discharges indicates that both the electron and ion diffusivities are independent of density. Discharges 77557 and 77559 represent a 1.0 MA, 2.0 T H mode neutral beam power scan at constant density [27]. Power balance analysis of these discharges indicates that both the electron and ion diffusivities increase with increasing temperature. At the half-radius the electron diffusivity increases as approximately $T_e^{3/2}$ and the ion diffusivity as T_i. The two H mode elongation scans (discharges 81499, 81507, 82183 and 82188) in the database were conducted to test predictions of improved fusion performances at higher elongation based on several global confinement scaling relations [28].

Discharges 84682 and 87031 are negative central shear (NCS) discharges with large and weak negative magnetic shear values, respectively, with both having an L mode edge [29, 30]. Unlike previous DIII-D contributions to the database, data for these two discharges contain a full time history of the profiles, including toroidal rotation.

3.4. FTU

The FTU tokamak [31] is an almost circular cross-section molybdenum limiter device with major radius $R = 0.93$ m, minor radius $a = 0.3$ m, and maximum design values of toroidal field and plasma current of $B_T = 8.0$ T and $I_p = 1.3$ MA, respectively. Auxiliary heating is provided by ECRH; the ECRH scheme is based on heating at the fundamental frequency, with perpendicular, low field side launch and ordinary polarization. At present the FTU contribution to the profile database consists of one discharge (No. 12658), in a scenario of ECRH during a current ramp-up phase [32]. The discharge parameters are $B_T = 5.4$ T, $I_p = 0.3{-}0.5$ MA, volume averaged electron density $\langle n_e \rangle = (2{-}3) \times 10^{19}$ m^{-3}, $q_{95} = 9{-}5$ and $P_{ECRH} = 0.35$ MW, with the resonant magnetic field located at the plasma axis. A current ramp-up scenario is used to obtain inverted or flat q profiles by exploiting the skin effect enhanced by the high electron temperature. The peak electron temperature attains 7.5 keV; the ion temperature remains below 1.1 keV. The scenario is characterized by high Z_{eff} values ($Z_{eff} = 6.7$ in the pulse), due to the low density.

3.5. JET

JET [33] is a large tokamak which has achieved near break-even in DT operation. Initially the JET device did not have a proper divertor; nevertheless, H mode operation was possible when an X point was formed away from the flat limiter structure. The minor radius of the plasma in this configuration, Mark 0, was quite large: $a = 1.1$ m, with a major radius $R = 3.0$ m. Following the introduction of, first, the Mark I and then the Mark II divertor, the minor radius was reduced to $a = 0.9$ m and the major radius to $R = 2.9$ m. The range of parameters covered in the database is $1.0 < I_p(\mathrm{MA}) < 3.2$, $1.0 < B(\mathrm{T}) < 3.1$, line density $1.7 < n_e\,dl$ (10^{19} m^{-2}) < 7.34 and input power $2.0 < P$ (MW) < 18. The additional heating is provided by NBI and ICRH; LHCD is used for current drive. The geometrical shaping parameters lie in the ranges $1.42 < \kappa < 1.72$ and $0.03 < \delta < 0.43$.

A wide variety of discharges, 22 in total, has been included in the database. There are L modes, ELM-free H modes, ELMy H modes and optimized shear discharges. Scans of the dimensionless parameters ρ_*, ν_* and β are also included. Most discharges are with Inconel/carbon walls, a carbon/beryllium limiter and beryllium evaporation.

In the Mark 0 configuration there are two limiter deuterium discharges (Nos 19649 and 19691), evolving from the ohmic phase to L mode with NBI heating [34], and two hot ion modes (Nos 26087 and 26095) from the Preliminary Tritium Experiment

[35, 36]. These latter are in a single X point configuration with deuterium gas (one discharge, No. 26095, with a tritium trace) and NBI heating; the discharges evolve from L to H to VH mode. There are eight ELMy H mode discharges from the Mark I, pump divertor, single null X point configuration, in which the ion ∇B drift is towards the X point. The gas is deuterium (apart from discharge 32745 with 20% helium) and the heating NBI (apart from discharge 33131 with hydrogen minority RF heating, which reduces to 10% of the NBI heating when this is switched on). Five of these discharges (Nos 33131, 33140, 35156, 35171 and 35174) are from a series of ρ_* scaling experiments for ITER [37]; two others [38] include an H mode discharge with large ELMs and high β (No. 34340), suitable for ITER scaling.

In the Mark II divertor configuration, there are eight ELMy H mode discharges. The first six, which are NBI heated (apart from No. 37728 with ∼15% RF heating) and mainly deuterium gas (but with up to 20% helium present), form a group [39]. Two discharges (Nos 37379 and 37944) form part of the ρ_* scaling experiments, two more (Nos 37718 and 37728) are from ν_* scaling studies and the other two (Nos 38407 and 38415) from a series of β scaling experiments for ITER. The remaining two discharges are deuterium ELMy H modes, one (No. 38285) with high gas fuelling, the other (No. 38287) with low gas fuelling [39]; these are dominantly NBI heated, but with 20% RF heating.

Finally there are two discharges in the standard scenario for high performance optimized shear operation, both in deuterium in the Mark IIap divertor configuration. The requisite q profiles are formed by a fast current ramp and early X point formation, followed by LHCD. In the first discharge (No. 40542) [40–42], NBI heating is then applied, leading to the formation of an ITB in L mode; this then evolves to develop an ELMy H mode edge transport barrier, and approaches steady state conditions. The second discharge (No. 40847), [41–43] which achieved the second highest neutron rate in JET deuterium discharges, involved modest ICRH hydrogen minority preheating; after NBI heating an L mode with an ITB formed, but this evolved to an ELM-free H mode edge which persisted until the first ELM led to an ELMy H mode phase, during which the performance progressively deteriorated.

3.6. JT-60U

JT-60U [44–46] is a large tokamak with major radius $R < 3.5$ m, minor radius $a < 1.1$ m, toroidal field $B_T < 4.4$ T and elongation $\kappa < 1.8$. In the original open divertor configuration the machine had a plasma current $I_p < 5.0$ MA and the neutral beam power was $P_{NBI} < 37$ MW. The open divertor configuration was modified to a W shaped semiclosed divertor configuration with a divertor pumping system in 1997 (from discharge E28748 onwards). This enhanced the control of heat, particles and impurities in the divertor region. A variety of auxiliary heating methods such as NBI and IC, LH and EC RF waves enable the flexible control of heating and current drive profiles.

A total of nine discharges have been contributed to the profile database. The ranges of parameters covered in the database are $R = 3.19{-}3.33$ m, $a = 0.80{-}0.96$ m, $B_T = 2.41{-}4.21$ T, $I_p = 1.00{-}3.51$ MA and $\kappa = 1.41{-}1.65$, while the heating power is in the range $P = 5.29{-}21.13$ MW. All these discharges are heated by NBI. Most of the discharges in the database have one time slice profile; the exceptions are discharges E16107 (six time slices) and E16168 (25 time slices). Two pairs of L mode discharges (Nos E21795, E21810 and E21796, E21811) were adopted for the study of the ρ_* dependence of confinement and transport [47]. The multitime profiles, including L to H and H to L transitions (discharges E16107 and E16168), show evidence of the non-local nature of transport variation at the transitions [48]. The relation between reduced transport with ITBs and the radial electric shear has been analysed from profiles of reversed shear plasmas with parabolic type ITBs (discharge E29390) and box type ITBs (discharges E29728 and E32423); discharges E29390 and E32423 are described in Ref. [49] and discharge E29728 in Ref. [50].

3.7. RTP

The RTP tokamak was a circular limiter tokamak with $R_0 = 0.72$ m, $a = 0.164$ m, $I_p \leq 150$ kA and $B_T \leq 2.4$ T, equipped with 350 kW of ECRH power, which can be deposited on- and off-axis in a very narrow region ($<0.1a$) [51]. It should be noted that RTP has very good electron diagnostics, but no measurement of T_i. However, due to the weak electron–ion coupling, it is well suited for studying electron thermal transport. With off-axis ECRH, a regime with hollow T_e and reversed magnetic shear inside the power deposition radius r_{dep}, and a transport barrier just outside r_{dep}, can be obtained. The electron power balance inside r_{dep} yields χ_e close to, or even below, zero, indicating the existence of an outward convection term [52, 53]. An example of such

a discharge has been supplied to the profile database, together with an ohmic reference discharge.

3.8. T-10

T-10 is a circular cross-section limiter tokamak with major radius $R = 1.5$ m, aspect ratio ∼4 and maximum toroidal field $B_T = 4.5$ T. Discharges with ECRH were used for the profile database. These discharges were obtained in the 1988 experimental campaign. In these experiments it was found that the energy confinement time is proportional to plasma density [54]. The contribution consists of 40 time slices from 20 discharges. Two time slices are provided for each discharge: ohmic at 0.1 s before the ECRH start and L mode at the end of the ECRH; both are close to stationary state. The experiments were carried out using a circular graphite poloidal limiter with radius of 0.34 m and a movable graphite bottom rail limiter. The ranges of variation of the main plasma parameters are as follows: $0.153 < I_p$ (MA) < 0.428; $2.76 < B_T$ (T) < 3.07; $0.58 < P_{ECRH}$ (MW) < 1.89; $1.47 < \bar{n}_e(10^{19}$ m$^{-3}) < 5.59$ and $2.43 < q_{95} < 7.17$.

3.9. TFTR

TFTR was a large DT capable limiter tokamak [55, 56] with nearly circular cross section, major radius $R = 2.6$ m and minor radius $a = 0.9$ m. Most discharges were heated by neutral beams (up to 40 MW, typically at 95 to 115 keV) mostly operated with deuterium, but also with tritium in the DT campaign. Discharges in the profile database represent the following regimes: ohmic, L mode, H mode, supershot, radiating mantle and enhanced confinement reversed shear (ERS). Descriptions of many of the TFTR discharges in the profile database can be found at http://www-local.pppl.gov/database.

Four discharges with hydrogen minority ICRF heating — but no neutral beam heating — (Nos 88643, 88659, 88956 and 88964) form an L mode DT isotope scan (scan Iso3) [57]. A four discharge power scan [58] at constant density (discharges 42290, 42292, 43020 and 43480) was produced by using helium puffs to reduce the confinement to L mode. There is no direct measurement of the helium content so its density is estimated from the measured change in the neutron rate. Current ramp scan Ip1 is composed of neutral beam heated L mode discharges [59, 60] (ramp duration from 0.3 to 1.0 s) and it includes a scan of pre-ramp densities from 3.7×10^{19} to 7.3×10^{19} m^{-3} (discharges 45950, 45966, 45980, 45984, 46290, 46291, 52179, 52182–84, 52186–88, 52194 and 52233). Dimensionless scaling [59] of L mode plasmas was investigated with a collisionality scan (discharges 50862, 50903 and 52527) and a ρ_* scan (discharges 50904, 50911 and 50921). The TFTR tangentially oriented neutral beams could inject in the direction of the plasma current (co-injection) and in the opposite direction (counter-injection). This enabled TFTR to conduct a high power co-/counter-injection scan experiment at ∼12 MW [62]. The discharges are in two groups with different magnetic field strengths: discharges 105290–105324 have $B_T = 4.8$ T, $I_p = 2.0$ MA, while discharges 105338–105353 have $B_T = 2.4$ T, $I_p = 1.0$ MA. Neutral beam heated DT isotope scans were carried out in L mode [63]; see scan Iso1: discharges 88574, 88578, 88582, 88615, 88720 and 88742. These discharges also include a power scan and a balanced versus all co-injection comparison.

A low recycling deuterium supershot plasma (discharge 55851) has been thoroughly documented [64]. Various DT supershots are provided: the first high fusion power DT supershot 73268 (and a deuterium-only comparison, No. 73265) [65], and a higher fusion power DT supershot (No. 76770) [64]. The beam heated Iso2 scan [67–69] is a DT isotope scan and a power scan (3–22 MW) of supershot plasmas (discharges 79005, 79010, 79013, 79014, 79021, 79023, 79084, 79097, 79099, 79100, 79119 and 79121). All discharges are at $R/a = 2.52/0.87$ m, 4.75 T, 1.6 MA. This scan captures two characteristic features of supershot plasmas — the favourable dependence of χ_i on heating power (or T_i) in the core, and the strongly favourable isotope scaling. The net beam direction varies from exactly balanced injection to co-dominated injection (co-dominated injection generally yields somewhat higher energy confinement time τ_E), and so this scan also provides some information on the correlation of toroidal rotation with transport. Two discharges (Nos 76535 and 76539) were part of the first experiments to measure helium ash accumulation [70]. These are representative of moderately good supershot performance. Discharge 76535 is heated by pure deuterium NBI, while discharge 76539 has a mix of deuterium and tritium. At 3.85 s, these discharges have very similar density profiles and similar total stored energy. However, slightly more power was required in the deuterium NBI discharge (27 MW) than in the DT NBI discharge (24 MW), and the DT discharge also has considerably higher central ion temperature, 28 versus 21 keV, which is typical of the isotope effect in

supershot plasmas; note that the beam power was stepped down after 4.1 s. Isotope scaling of confinement in the high-l_i type supershots [71] is evident in discharges 84242, 84243 and 95554, 95555. Supershots with radiating mantles [72] were created by puffing krypton (discharges 103646, 103648 and 103649) and xenon (discharges 103808–103810). The radiated power fraction rises to approximately 100% without significantly reducing either the electron or ion temperature profiles.

H mode plasmas in TFTR are complementary to those in other tokamaks, in that the density profile is quite peaked. The first high heating power (>20 MW) and resulting high DT fusion power (>6.7 MW) H modes were obtained during the DT campaign on TFTR. The discharges provided (Nos 74897, 74898, 77780 and 77801) are from a study of D/T isotope differences [73, 74].

The canonical ERS mode [75] discharge (No. 84011) is provided. Loss of an ITB in the ERS regime is documented [76] in scan ERS-2 (discharges 94599, 94601, 94603, 94604 and 94607). The relaxation of core transport barriers was studied by varying the radial electric field using different applied torques from NBI.

Two supershot discharges, No. 91472 (R = 2.59 m, 1.8 MA, 26 MW) and No. 102257 (R = 2.45 m, 1.6 MA, 22 MW), exhibit time dependent perturbations caused by a sudden increase in radiative cooling and subsequent serious deterioration in energy confinement. Reference [77] provides background on the phenomena known as 'carbon blooms. Supershot degradation due to helium puffing is documented [78] in discharges 61195 (an unperturbed supershot) and 61206 (a supershot with helium gas puff). The helium puff causes a factor ~2 reduction in τ_E within 100–150 ms. Kinetic transport analysis indicates that the core ion thermal diffusivity increases substantially, about a factor of 3–4. Perturbations of supershots by gas puffing or pellet injection [59] are seen in scan SS1 (discharges 43162, 43812, 44647, 44660, 44665 and 44669). Cold pulse propagation can be studied in scan CP1 [79, 80] which is comprised of three ohmic discharges (Nos 79006, 79169 and 89168) and one supershot (No. 83526) in which a temperature perturbation was observed; the perturbation is presumed to be caused by an infalling carbon flake. Note that the ion temperature provided for the ohmic discharges is calculated by TRANSP (no CHERS data are available without neutral beam heating).

3.10. Tore Supra

Tore Supra is a circular device with major radius R = 2.4 m and minor radius a = 0.8 m [81]. The experiments have been carried out using either LHCD or ICRH, at the following plasma parameters: $0.4 \leq I_p$ (MA) ≤ 1.5, $2.1 \leq B_T$ (T) $\leq 3.7, 1.7 \leq \bar{n}$ (10^{19} m^{-3}) ≤ 4.7, where $\bar{n}$ is the line averaged density. The working gas is normally helium although one discharge (No. 23418) is in deuterium. The ICRH heating scheme is either hydrogen minority or direct fast wave electron heating (FWEH): the total additional power $P_{Tot} < 10$ MW ($P_{ICRH} < 9$ MW, $P_{LHCD} < 3$ MW). Electron heating is dominant during RF application, i.e. T_e is much higher than T_i (up to $4T_i$). For LHCD and FWEH discharges, more than 90% of the RF power is coupled to the electrons. The ions are weakly heated by equipartition. The discharges submitted to the database comprise L mode [82], LHCD with ITBs [83] and FWEH with high magnetic shear [84].

3.11. TEXTOR

TEXTOR is a medium size tokamak with circular cross-section, which is equipped with two poloidal limiters and one toroidal limiter [85]. The major radius of TEXTOR is R = 1.75 m and the minor radius of the discharges can vary between a = 46 cm and about 40 cm, depending on the positioning of the poloidal and/or toroidal limiters. Auxiliary heating on TEXTOR consists of ICRH and NBI. Two neutral beam injectors are installed, one co-beam and one counter-beam, capable of delivering up to 2 MW at a maximum of 60 kV each. The injectors can be operated with hydrogen, deuterium, ^{3}He and ^{4}He. The ICRH system consists of two antenna pairs, fed by two separate generators capable of delivering 2 MW each. Values for the toroidal magnetic field B_T and plasma current I_p are: $1.6 < B_T$ (T) < 2.6 and $200 < I_p$ (kA) < 520. An I mode discharge is in the database [86]. A pair of corresponding discharges, one in RI mode (No. 68803) and one in L mode (No. 68812), have been processed and will be contained in the next public release of the database.

4. Analysis of data ranges available

It is helpful to analyse the range of data covered by the discharges in the database. Figure 1 shows the range of various plasma parameters (i.e. a, R, n, B_T, I_p and Z_{eff}) and geometrical parameters (i.e. q_{cyl}, a/R and κ). The notation is such that the box shows

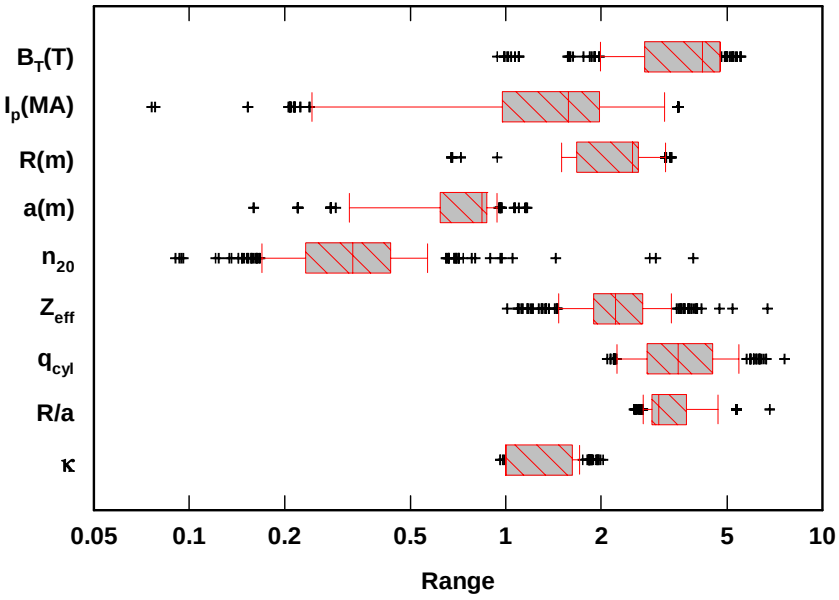

Figure 1. Ranges of magnetic field B_T, toroidal current I_p, major radius R, minor radius a, line averaged electron density normalized to 10^{20} m^{-3}, n_{20}, effective charge Z_{eff}, cylindrical safety factor q_{cyl}, aspect ratio R/a and elongation κ.

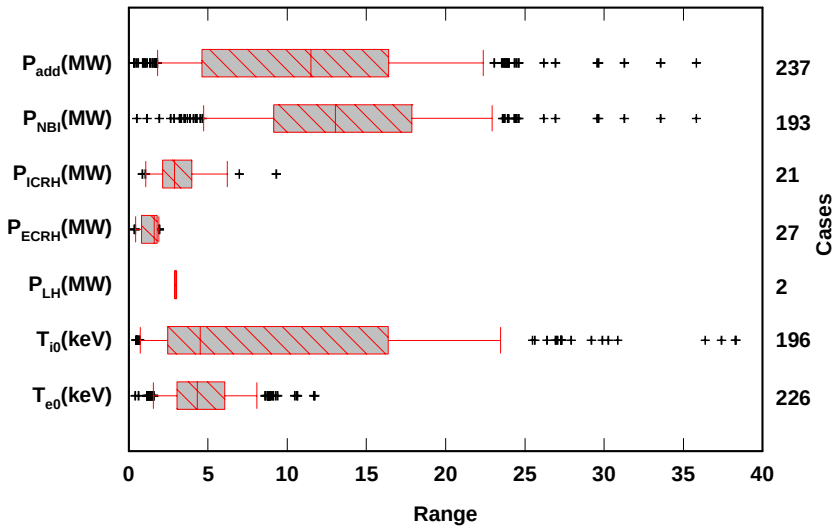

Figure 2. Ranges of total additional power P_{add}, NBI power P_{NBI}, ICRH power P_{ICRH}, ECRH power P_{ECRH} and LH power P_{LH}, and the axial ion and electron temperatures, T_{i0} and T_{e0}, respectively. The number of cases in each data set is indicated. Some cases have more than one power source at the reference time.

the region containing the middle 50% of the data points, i.e. from 25 to 75%; the vertical bar inside the box is the median; and the vertical lines outside the box are at 10 and 90%. All outliers (upper and lower 10% of the data) are designated by + signs.

As reflected in the ranges of the geometrical parameters, data from the large tokamaks dominate the database; 32 from DIII-D, 24 from JET, 38 from JT-60U, and 111 from TFTR, or 205 of the 265 cases. The middle 80% of the data for κ, R/a, a and R

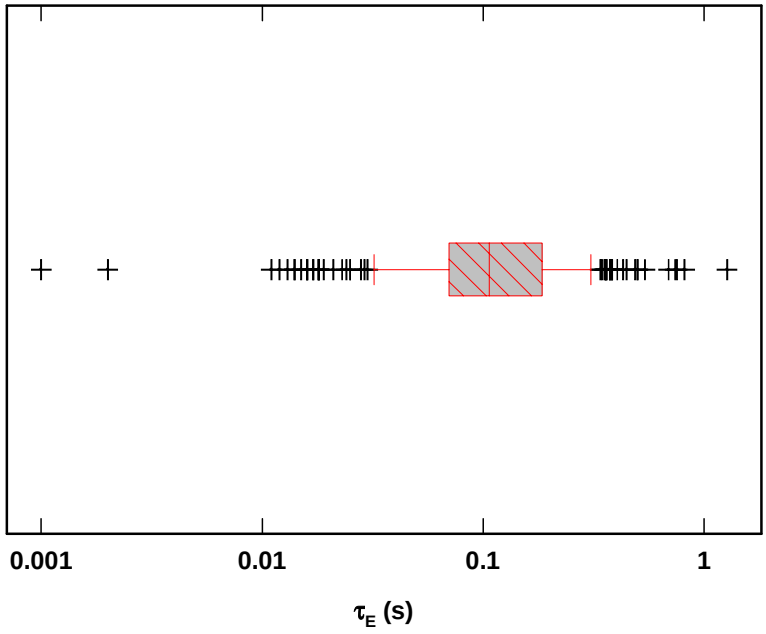

Figure 3. Range of global thermal energy confinement time, τ_E (s).

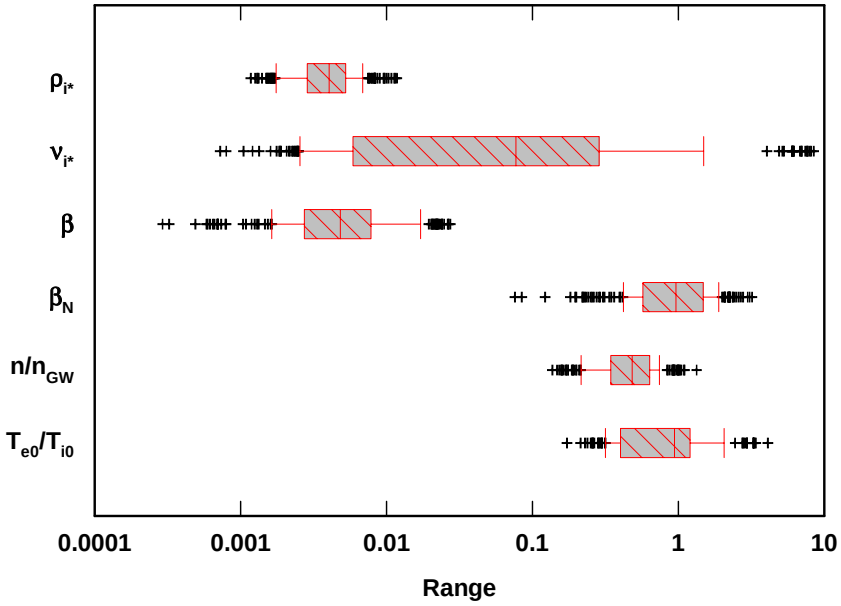

Figure 4. Ranges of ion gyroradius normalized to the system size ρ_{i*}, effective collisionality normalized to the bounce frequency ν_{i*}, toroidal plasma beta β, normalized plasma beta β_N, line averaged electron density normalized to the empirical Greenwald density limit n/n_{GW} and ratio of axial electron to ion temperatures T_{e0}/T_{i0}. The temperatures used to evaluate the collisionality and gyroradius expressions are characteristic of the middle portion of the profile.

therefore represents those machines, and the skewing of the median towards either end of the box is due to half of these data being from TFTR. The plasma parameters show a wider range of variation, reflecting the attempts to include scans of density, current and toroidal magnetic field from each device. It is noteworthy that density and plasma current show the widest range of variation.

A similar presentation is used in Fig. 2 for the additional power P_{add} and axial temperatures T_{io} and T_{eo} that result; this figure also analyses the type of heating employed: P_{NBI}, P_{ECRH}, P_{ICRH} and P_{LH}. About 90% of the cases include some form of additional heating. Although a few cases have more than one source of additional heating, NBI is predominant. Because charge exchange recombination spectroscopy is the most common means of measuring ion temperature and requires NBI, there are very few cases without beam injection that include ion temperatures. Therefore, selection of a subset of data for testing two fluid transport models will usually be dominated by discharges with neutral beam heating. The axial temperatures show that the ion temperatures can be generally much greater than the electron temperatures. However, the median values are nearly the same, and the lower 10% of the ion temperatures is nearly a factor of two lower than the electron temperatures. The higher ion temperatures reflects the dominance of ion heating from NBI more than it reflects relative transport properties of ions and electrons. At low temperatures ohmic heating of electrons is dominant.

The ensuing range of global thermal energy confinement times τ_E is displayed in Fig. 3. Although the entire range covers three orders of magnitude, the middle 80% covers only one order of magnitude, and the middle 50% of the data falls between 60 and 200 ms with a median value at 100 ms.

It is also helpful to present the various dimensionless plasma parameters (i.e. ρ_{i*}, ν_{i*}, β, β_N (normalized plasma beta), n/n_{GW} and T_{e0}/T_{i0}) shown in Fig. 4. When plotted this way it is surprising to note that nearly 50% of the cases that report both electron and ion temperatures have $T_{e0} \geq T_{i0}$. These represent most of the cases that are not dominated by beam injection and the lower end of the temperature range, although there is a significant number of cases with several MWs of beam injection that fall into this category. Plasma collisionality ν_{i*}, evaluated at a mean temperature and density representing the middle of the profile, spans more than four orders of magnitude. Half of the β_N values exceed unity and have a range comparable to the average plasma beta values. Although they represent two of the more critical parameters for scaling to fusion plasmas and a devoted effort has been made to extend their ranges, the smallest data ranges are covered by the dimensionless ion gyroradius, ρ_{i*}, and density scaled to the Greenwald limit, n/n_{GW}. There are eight TFTR 1 MA cases and one Tore Supra case that equal or exceed the Greenwald limit.

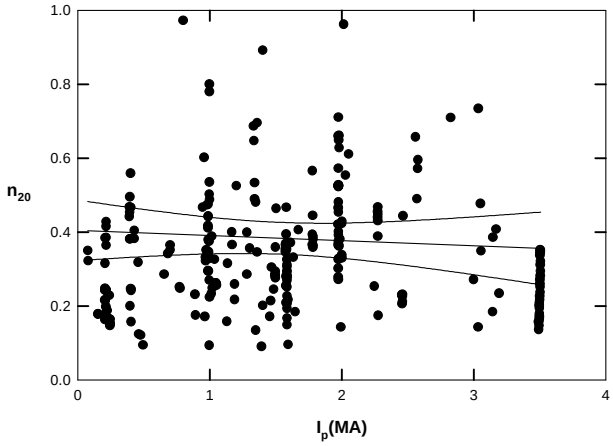

Figure 5. Absence of correlation between the line averaged electron density n_{20} and the plasma current I_p in the database; there are some obvious density scans at constant current.

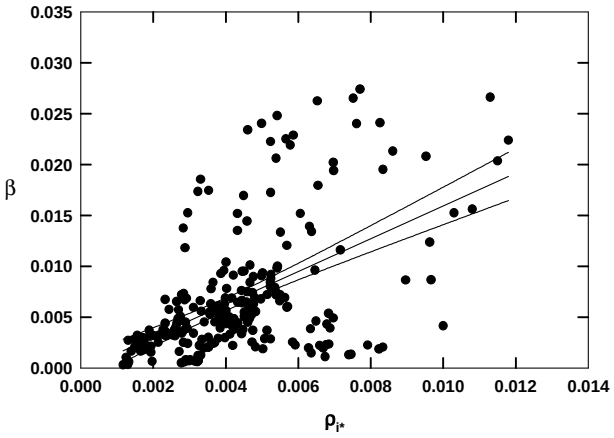

Figure 6. Weak correlation between β and ρ_{i*}; however, the lowest ρ_{i*} cases are all at low β.

In order to investigate how well conditioned the database is we sought possible correlations. Figure 5 shows no evidence for correlation between n and I_p (the figure indicates clear density scans at constant current). In this figure the centre line shows a linear regression fit and the upper and lower lines span the 95% confidence interval. Considering dimensionless

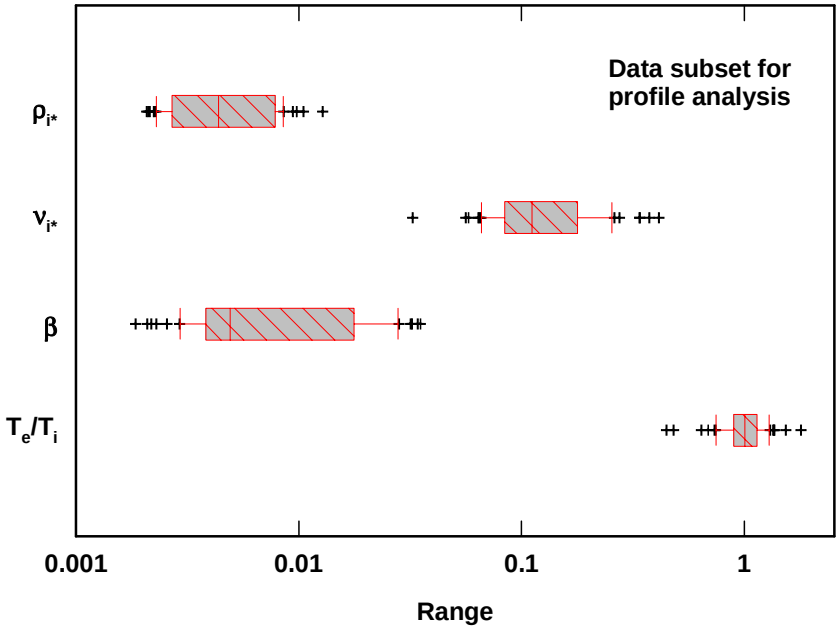

Figure 7. Ranges of dimensionless parameters at the mid-minor radius ($\rho = 0.5$) for a selection of 59 cases that satisfy data completeness requirements for local transport analysis.

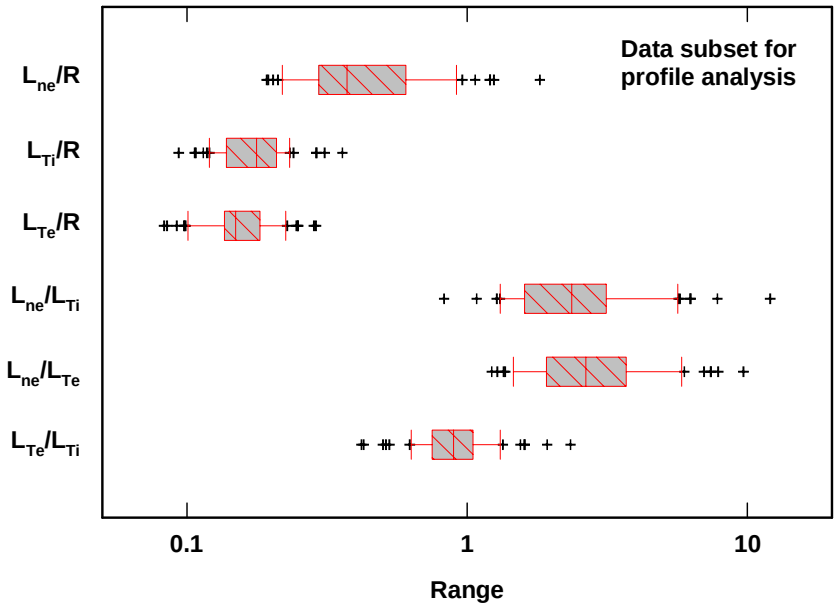

Figure 8. Ranges of dimensionless scale lengths at the mid-minor radius ($\rho = 0.5$) for a selection of 59 cases that satisfy data completeness requirements for local transport analysis. The parameters that depend on the density gradient scale length for two cases with slightly inverted density profiles (large negative L_{ne}) are not shown.

parameters, there is little evidence for a correlation when beta is plotted versus ρ_{i*} as in Fig. 6. Again the three lines indicate a linear regression fit and the 95% confidence interval. When beta is plotted versus $1/\rho_{i*}$, a tail of low β values at the lowest ρ_{i*} appears; these are essentially all TFTR L mode data.

A selection of 59 cases has been made from the profile data for the purpose of testing local transport models [12]. The criteria for selection include completeness of profile information and source terms, nearness to steady state, etc., for the selected time slices. Figure 7 shows that the dimensionless parameters for these cases, at the mid-plasma-radius, each span about an order of magnitude. The electron to ion temperature ratio actually has the narrowest ranges (i.e., both for the total and for the middle 50% of the data). The dimensionless gradient scale lengths relevant for testing many turbulence models, (i.e. L_{ne}/R, L_{Ti}/R, L_{Te}/R, L_{ne}/L_{Ti}, L_{ne}/L_{Te} and L_{Te}/L_{Ti}), are shown in Fig. 8; the widest range is in the density scale length (two cases with inverted density profiles are not shown for clarity). Although the electron temperature scale length has the narrowest range, it does not reflect excessive rigidity. A possible correlation between the plasma thermal beta and dimensionless ion gyroradius is examined in Fig. 9. Although there appears to be linear upper and lower bounds (the data would appear as a band in a log–log plot), almost all the data at the lowest end are dominated by cases from a single machine (TFTR). This could introduce a geometric bias in the data, which can be reduced by obtaining a broader spectrum of cases from all machines.

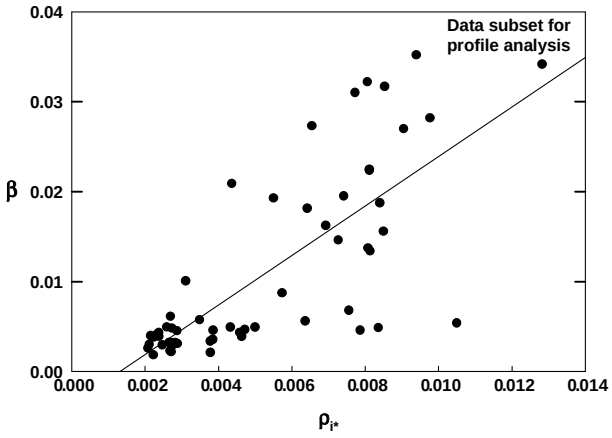

Figure 9. For the subset of data selected for detailed transport profile analysis (59 cases) there appears to be a linear upper bound in the relationship between β and ρ_{i*}. The cluster of data at the lower end is almost entirely from TFTR, so caution must be exercised in its interpretation.

5. Application to model testing

The International Profile Database provides a unique resource for testing transport models against reliable and well documented data from a variety of tokamaks, confinement modes and heating methods. The ITER Confinement and Database Expert Group have used the database in just this way [11–13] and in this section we present an illustrative example of this use of the database. For this purpose a number of features were developed to facilitate model testing in a systematic manner. These include standard forms for the 1-D transport equations into which models can be inserted, and standard formats for describing the models themselves. A set of 'figures of merit' for analysing the performance of models was agreed by the expert group. This has allowed the group to assess the validity of any particular model and judge the value of predictions using it for next step devices, such as ITER. Also, for these particular tests, a subset of discharges was selected that conformed to a stringent set of criteria, i.e. reasonably stationary in time at a selected time point and with a fairly complete set of variables available, including a measured ion temperature profile. Other discharges in the database are nevertheless of value for specific purposes, possibly unconnected with transport model testing.

In Table 5 we list the 12 transport models tested by the expert group, including the physics bases of the models and the names of those modellers who have tested them.

The standard subset of the profile database was divided into L mode and H mode discharges and the performance of the models against a particular figure of merit calculated for the two subsets, comprising 55 discharges in total. The figure of merit chosen is based on the incremental thermal stored energy W_{inc}, which is the energy above any 'edge pedestal energy' [13]; thus this takes no credit for using the edge temperature as a boundary condition (at $\rho = 0.9$) in obtaining the temperature profiles. Figure 10 shows the resulting comparisons for the RMS error in W_{inc} for the 12 models [12]; however, the discrimination is not decisive. A full discussion of these results can be found in Ref. [13]. They are presented here simply to illustrate how the profile database can be utilized. Much work remains to be done in using suitable figures of merit and other tests

Table 5. Models and modellers

Model	Modeller	Physics
Weiland	J. Weiland (EU), D. Mikkelsen (US), R. Waltz (US)	ITG
Multimode	J. Kinsey (US), G. Bateman (US), D. Mikkelsen (US)	Drift waves, RBM, kinetic ballooning, neoclassical
Waltz GLF23	R. Waltz (US), J. Kinsey (US)	ITG
IFS/PPPL, no $\boldsymbol{E} \times \boldsymbol{B}$;	M. Turner (EU), S. Attenberger (US), B. Dorland (US), D. Mikkelsen (US),	ITG
IFS/PPPL, $\boldsymbol{E} \times \boldsymbol{B}$	R. Waltz (US), Y. Ogawa (JA), D. Boucher (JCT)	ITG
CDBM	A. Fukuyama (JA), S. Attenberger (US), D. Mikkelsen (US), R. Waltz (US), D. Boucher (JCT), J. Kinsey (US), Y. Ogawa (JA)	Current diffusive ballooning modes
RLWB, RLW	D. Mikkelsen (US), D. Boucher (JCT)	Semi-empirical
Culham	M. Turner (EU), S. Attenberger, D. Boucher (JCT)	Semi-empirical
Mixed shear	G. Vlad/M. Marinucci (EU), D. Boucher (JCT), Y. Ogawa (JA)	Semi-empirical
T11/SET	A. Polevoi (RF)	Semi-empirical
CPTM	Yu. Dnestrovskij (RF)	Semi-empirical

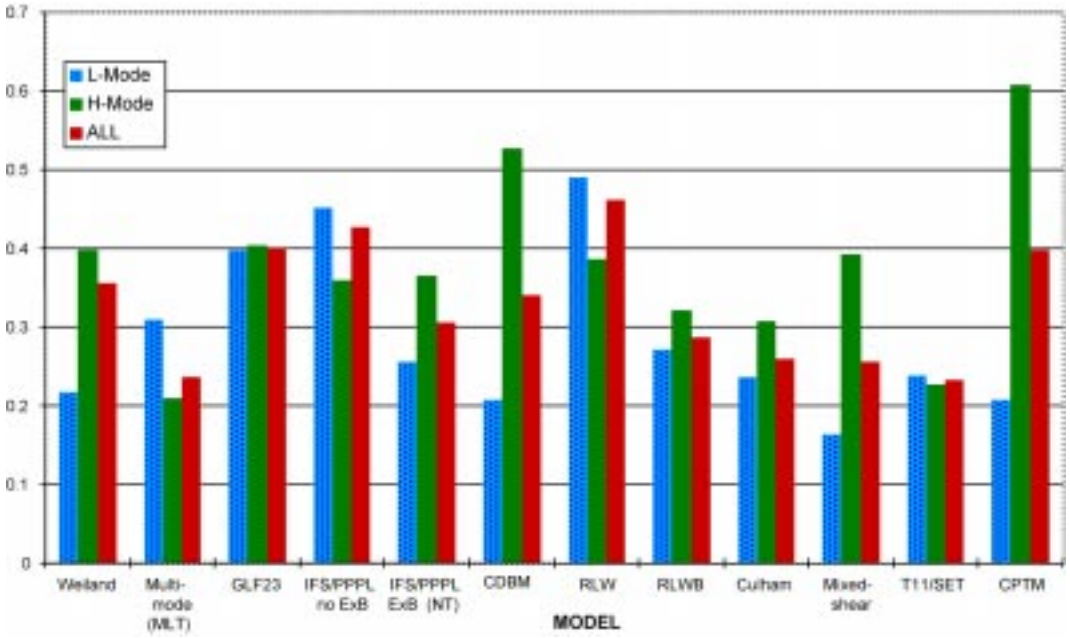

Figure 10. RMS of error in incremental stored energy W_{inc}, simulated by the 12 transport models for the subset of 55 discharges which have measured ion temperatures.

to discriminate better between the performance of the models.

6. Conclusions

This article has described the International Profile Database, which is now available to the fusion community electronically at its present home in the ITER JCT, Naka, Japan and may be accessed by anonymous ftp to iterphys.naka.jaeri.go.jp. The principal use of this database is to allow comprehensive testing of 1-D transport models in a systematic and open manner, although it may also be useful for other specific applications. The aim of the article has been to describe the nature of the database and its contents and how to access and use it, so that the fusion community as a whole can make full use of this valuable resource which has resulted from the efforts of workers on many tokamaks.

The Introduction explained the motivation for the construction of the database and also briefly described its basic arrangement. Section 2 described the structure in more detail. Because the principal purpose of the database is to provide a vehicle for transport model testing, it is important that the necessary variables for this are available in the database. The relevant general forms of the 1-D power and particle balance equations are presented in this section, identifying the various flux surface averaged quantities needed: e.g. T_i, T_e, n and various geometrical quantities derived from the equilibrium solution such as $\langle|\nabla\rho|^2\rangle$ and V'. The principal variables are listed and defined in Appendix A (for 0-D variables), Appendix B (for 1-D variables) and Appendix C (for 2-D variables). Appendices D, E and F, respectively, give examples of 0-D, 1-D and 2-D file formats for these variables. For those who need more detailed information on the database, a fully documented reference manual is available electronically from the database server.

In Section 3, summary descriptions of the character and parameters of contributing tokamaks, together with the types of discharge their data providers have submitted to the database, are given. These contributing tokamaks are ASDEX Upgrade, Alcator C-Mod, DIII-D, FTU, RTP, JT-60U, JET, T-10, TFTR, Tore Supra and TEXTOR, encompassing a wide range of parameters, shapes and heating methods. Furthermore, there is a considerable variety of discharge types: ohmic, L mode, H mode (ELM-free and with large and small ELMs), supershots, hot ion modes, hot electron modes, high power DT, optimized shear (ERS and NCS with ITBs), impurity injection and RI modes, and cold pulse experiments.

Section 4 provides a table of the global parameters in the database and plots showing the parameter spaces for various dimensionless variables, e.g. plasma physics ones: ρ_*, ν_*, β, T_e/T_i, M, n/n_{GW}; geometrical ones: q_{95}, R/a, κ, δ; and compositional ones: A_i, Z_{eff}; as well as dimensional ones: I, B, n, P, a. The relation of these to the values anticipated for ITER is discussed. Some limited information on profile characterization, e.g. R/L_T, R/L_n, L_n/L_T at $r = a/2$, is also given.

Finally, in Section 5 some example results from using the database for model testing are presented. This activity is ongoing as models evolve (sometimes in response to the results of the testing procedure!). At present, while these results show that some models perform somewhat better than others in representing the experimental data, there is a need to devise more discriminating tests, such as examining whether the performance of models varies systematically with parameters, e.g. ρ_* [12], or exploiting transient experiments [87]. Thus, unlike the situation with global databases, when one can deduce a scaling relation for a global confinement time, it is impossible to present a particularly meaningful single result from analysis of the profile database. Some transport model predictions (e.g. the ITG models in Refs [4, 5]) are sensitive to the temperature at the edge of the tokamak which serves as a boundary condition for simulations of the core transport; this is usually taken as an experimental input for model comparisons. To provide predictions for a next step device one would need to develop a model or scaling for this edge temperature, which in H mode is taken as the temperature at the top of the edge transport barrier, i.e. the 'pedestal' temperature. A database of pedestal parameters to assist in this is being developed [88].

It is anticipated that the International Profile Database will continue to expand. A priority is to include more discharges with an ITB present, such as optimized shear ones. Modelling of these, and other improved confinement modes, often requires information on radial electric field shear [89], which suppresses transport in some models (e.g. Refs [4, 5, 7]. It will be important to include such information in the database, but obtaining it is difficult, requiring modelling of plasma flows (e.g. based on neoclassical theory [90]). The ongoing interaction between modellers and the database within the 1D Modelling Working Group will indicate any need for more

information to be provided as a matter of necessity, rather than as 'additional' information. For example, in the future this could include equilibrium reconstructions based on EFIT [91], 1-D waveforms for gas puffing or pellet fuelling, statements on whether inside or outside launch of pellets is used and whether the ion ∇B drift is towards or away from an X point in single null configurations. The Working Group is also exploring the possibility of changing the form of the database to a format allowing the user to read and search.

In conclusion it is hoped that the description given here will help and encourage 1-D transport modellers to use this facility for testing their models.

Appendix A

Definitions of 0-D variables

Variable number	Variable name	Variable definition	Units
General			
1	TOK	Tokamak (10 ASCII characters)	
2	UPDATE	Most recent update YYMMDD	
3	DATE	The date the shot was taken. The format is YYMMDD	
4	SHOT	The shot from which the data are taken	
5	TIME	Time during the shot	s
6	AUXHEAT	Type of auxiliary heating (e.g. NB and EC)	
7	PHASE	The phase of the discharge at TIME (e.g. OHM, L and HSELM)	
8	STATE	Description of the plasma state (STEADY or TRANS)	
Plasma composition			
9	PGASA	Mass number of the plasma working gas	
10	PGASZ	Charge number of the plasma working gas	
11	BGASA	Mass number of the neutral beam gas	
12	BGASZ	Charge number of the neutral beam gas	
13	BGASA2	Mass number of the second neutral beam gas (JET only)	
14	BGASZ2	Charge number of the second neutral beam gas (JET only)	
15	PIMPA	Mass number of the plasma main impurity	
16	PIMPZ	Charge number of the plasma main impurity	
17	PELLET	Pellet material if a pellet(s) has been injected	
Geometry			
18	RGEO	Plasma geometrical major radius	m
19	RMAG	Major radius of the magnetic axis	m
20	AMIN	Horizontal plasma minor radius	m
21	SEPLIM	Distance between the separatrix and limiter	m
22	XPLIM	Distance between the X point and limiter	m
23	KAPPA	Plasma elongation	
24	DELTA	Triangularity of the plasma boundary	
25	INDENT	Indentation of the plasma	
26	AREA	Area of plasma cross-section	m^2
27	VOL	Plasma volume	m^3
28	CONFIG	Plasma configuration (e.g. single null, double null, limiter position)	
29	IGRADB	For CONFIG = SN, ion NB drift direction	

Appendix A (cont.)

Variable number	Variable name	Variable definition	Units
Machine conditions			
30	WALMAT	Material of the vessel wall	
31	DIVMAT	Material of the divertor tiles	
32	LIMMAT	Material of the limiters	
33	EVAP	Evaporated material used to cover inside of vessel	
Magnetics			
34	BT	Vacuum toroidal magnetic field at RGEO	T
35	IP	Plasma current	A
36	VSURF	Loop voltage at the plasma boundary	V
37	Q95	Plasma safety factor at 95% flux surface	
38	BEPMHD	Poloidal beta	
39	BETMHD	Toroidal beta	
40	BEPDIA	Corrected poloidal diamagnetic beta	
Densities			
41	NEL	Central line averaged electron density	m^{-3}
42	DNELDT	Time rate of change of NEL	m^{-3} s^{-1}
Impurities			
43	ZEFF	Line averaged plasma effective charge	
44	PRAD	Total radiated power	W
Input powers			
45	POHM	Total ohmic power	W
46	ENBI	Neutral beam energy weighted by power	V
47	PINJ	Injected neutral beam power	W
48	BSOURCE	Beam power fractions	
49	PINJ2	The injected beam power from the second source	W
50	BSOURCE2	The power fractions injected by the second beam	
51	COCTR	Fraction of beam power co-injected	
52	PNBI	Beam power less shinethrough	W
53	ECHFREQ	ECH frequency	Hz
54	ECHMODE	Mode of ECH waves	
55	ECHLOC	Location of ECH launch	
56	PECH	ECH power	W
57	ICFREQ	Frequency of ICRH waves	Hz
58	ICSCHEME	ICRH heating scheme	
59	ICANTEN	Antenna phasing	
60	PICRH	ICRH power	W
61	LHFREQ	Frequency of LH waves	Hz
62	LHNPAR	LH parallel mode number	
63	PLH	LH power	W
64	IBWFREQ	Frequency of IBW	Hz
65	PIBW	IBW power	W
Temperatures			
66	TE0	Electron temperature	eV
67	TI0	Ion temperature	eV

Appendix A (cont.)

Variable number	Variable name	Variable definition	Units
Energies			
68	WFANI	Fraction of fast ion energy due to NBI in perpendicular direction	
69	WFICRH	Perpendicular fast ion energy content during ICRH	J
70	MEFF	Effective atomic mass	amu
71	ISEQ	Parameter scan identifier	
72	WTH	Thermal plasma energy	J
73	WTOT	Total plasma energy	J
74	DWTOT	Time rate of change of WTOT	J s^{-1}
75	PL	Loss power (uncorrected)	W
76	PLTH	Loss power (corrected)	W
77	TAUTOT	Total energy confinement time	s
78	TAUTH	Thermal energy confinement time	s

Appendix B

Definitions of essential 1-D variables

Variable number	Variable name	Variable definition	Units
1	IP	Plasma current	A
2	BT	Vacuum toroidal magnetic field at RGEO	T
3	AMIN	Horizontal plasma minor radius	m
4	RGEO	Plasma geometrical major radius	m
5	KAPPA	Plasma elongation	
6	DELTA	Triangularity of the plasma boundary	
7	INDENT	Indentation of the plasma	
8	PNBI	Total injected neutral beam power minus shinethrough	
9	PECH	ECH power coupled to the plasma	W
10	PICRH	ICRH power coupled to the plasma	W
11	PLH	LH power coupled to the plasma	W
12	PIBW	IBW power coupled to the plasma	W
13	PFLOSS	Amount of neutral beam power lost from the plasma through charge exchange and unconfined orbits	W
14	PRAD	Total radiated power	W
15	ZEFF	Line averaged plasma effective charge	
16	NEL	Line averaged electron density	m^{-3}

Appendix C

Definitions of the most commonly provided 2-D variables

Variable number	Variable name	Symbol*	Variable definition	Units
1	TE	T_e	Fitted electron temperature profile	eV
5	TI	T_i	Fitted ion temperature profile	eV
9	NE	n_e	Fitted electron density profile	m^{-3}
13	QNBIE	Q_e	Power deposition profile on thermal electrons by beams	W m^{-3}
14	QICRHE	Q_e	Power deposition profile on thermal electrons by ICRH	W m^{-3}
15	QECHE	Q_e	Power deposition profile on thermal electrons by ECH	W m^{-3}
16	QLHE	Q_e	Power deposition profile on thermal electrons by LH	W m^{-3}
17	QIBWE	Q_e	Power deposition profile on thermal electrons by IBW	W m^{-3}
18	QNBII	Q_i	Power deposition profile on thermal ions by beams	W m^{-3}
19	QICRHI	Q_i	Power deposition profile on thermal ions by ICRH	W m^{-3}
20	QECHI	Q_i	Power deposition profile on thermal ions by ECH	W m^{-3}
21	QLHI	Q_i	Power deposition profile on thermal ions by LH	W m^{-3}
22	QIBWI	Q_i	Power deposition profile on thermal ions by IBW	W m^{-3}
23	SNBIE	S_e	Source of thermal electrons from beams	m^{-3} s^{-1}
24	SNBII	S_i	Source of thermal ions from beams due to thermalization of beam particles	m^{-3} s^{-1}
25	CURNBI		Current drive profile by beams	A m^{-3}
26	CURICRH		Current drive profile by ICRH	A m^{-3}
27	CURECH		Current drive profile by ECH	A m^{-3}
28	CURLH		Current drive profile by LH	A m^{-3}
29	NFAST	n_i	Non-thermal ion density profile	m^{-3}
30	QRAD	$-Q_e$	Total radiated power density	W m^{-3}
32	ZEFFR		Plasma effective charge radial profile	
34	Q		Safety factor profile	
38	NM1	n_i	Main ion density profile	m^{-3}
42	NM2	n_i	Secondary main ion density profile	m^{-3}
42b	NM3	n_i	Third main ion density profile	m^{-3}
46	NIMP	n_i	Main impurity density profile	m^{-3}
50	QOHM	Q_e	Ohmic power density	W m^{-3}
52	CURTOT		Total current density	A m^{-3}
54	VROT		Fitted toroidal angular speed	s^{-1}
58	DWER	$\frac{\partial}{\partial t} W_e(\rho, t)$	Term of the electron energy conservation equation	W m^{-3}
59	DWIR	$\frac{\partial}{\partial t} W_i(\rho, t)$	Term of the ion energy conservation equation	W m^{-3}
60	DNER	$\frac{\partial}{\partial t} n_e(\rho, t)$	Term of the electron particle conservation equation	m^{-3} s^{-1}
61	SWALL		Main thermal ion particle source term due to ionization of recycling wall neutrals	m^{-3} s^{-1}
62	QWALLE	$-Q_e$	Thermal electron heat loss due to the ionization of wall neutrals	W m^{-3}
63	QWALLI	$-Q_i$	Main thermal ion heat loss due to ionization and charge exchange with wall neutrals	W m^{-3}
64	QFUSE	Q_e	Electron heating density due to DT fusion reaction	W m^{-3}
65	QFUSI	Q_i	Main thermal ion heating density due to DT fusion reaction	W m^{-3}
66	BPOL		Surface averaged poloidal magnetic field	T
67	RMAJOR		Geometrical major radius	m
68	RMINOR		Geometric minor radius of the magnetic surface at the elevation of the magnetic axis	m
69	VOLUME	V	Volume enclosed by the magnetic surface	m^3
70	KAPPAR		Averaged elongation of the magnetic surface	

Appendix C (cont.)

Variable number	Variable name	Symbol*	Variable definition	Units
71	DELTAR		Averaged triangularity of the magnetic surface	
72	INDENTR		Averaged indentation of the magnetic surface	
73	SURF		Surface area of the magnetic surface	m^2
74	GRHO1	$\langle\lvert\nabla\rho\rvert\rangle$	Geometric term of the particle and energy conservation equations	m^{-1}
75	GRHO2	$\langle\lvert\nabla\rho\rvert^2\rangle$	Geometric term of the energy conservation equations	m^{-2}

* Relevant term in the particle or energy transport equations.

Appendix D

Format of 0-D file

	Start byte						
Record	01	12	23	34	45	56	67
1	TOK A10,1X	UPDATE I10,1X	DATE I10,1X	SHOT I10,1X	TIME 1PE10.3,1X	AUXHEAT A10,1X	PHASE A10,1X
2	STATE A10,1X	PGASA I10,1X	PGASZ I10,1X	BGASA I10,1X	BGASZ I10,1X	BGASA2 I10,1X	BGASZ2 I10,1X
3	PIMPA I10,1X	PIMPZ I10,1X	PELLET A10,1X	RGEO 1PE10.3,1X	RMAG 1PE10.3,1X	AMIN 1PE10.3,1X	SEPLIM 1PE10.3,1X
4	XPLIM 1PE10.3,1X	KAPPA 1PE10.3,1X	DELTA 1PE10.3,1X	INDENT 1PE10.3,1X	AREA 1PE10.3,1X	VOL 1PE10.3,1X	CONFIG A10,1X
5	IGRADB I10,1X	WALMAT A10,1X	DIVMAT A10,1X	LIMMAT A10,1X	EVAP A10,1X	BT 1PE10.3,1X	IP 1PE10.3,1X
6	VSURF 1PE10.3,1X	Q95 1PE10.3,1X	BEPMHD 1PE10.3,1X	BETMHD 1PE10.3,1X	BEPDIA 1PE10.3,1X	NEL 1PE10.3,1X	DNELDT 1PE10.3,1X
7	ZEFF 1PE10.3,1X	PRAD 1PE10.3,1X	POHM 1PE10.3,1X	ENBI 1PE10.3,1X	PINJ 1PE10.3,1X	BSOURCE I10,1X	PINJ2 1PE10.3,1X
8	BSOURCE2 I10,1X	COCTR 1PE10.3,1X	PNBI 1PE10.3,1X	ECHFREQ 1PE10.3,1X	ECHMODE A10,1X	ECHLOC A10,1X	PECH 1PE10.3,1X
9	ICFREQ 1PE10.3,1X	ICSCHEME A10,1X	ICANTEN A10,1X	PICRH 1PE10.3,1X	LHFREQ 1PE10.3,1X	LHNPAR 1PE10.3,1X	PLH 1PE10.3,1X
10	IBWFREQ 1PE10.3,1X	PIBW 1PE10.3,1X	TEO 1PE10.3,1X	TIO 1PE10.3,1X	WFANI 1PE10.3,1X	WFICRH 1PE10.3,1X	MEFF 1PE10.3,1X
11	ISEQ A10,1X	WTH 1PE10.3,1X	WTOT 1PE10.3,1X	DWTOT 1PE10.3,1X	PL 1PE10.3,1X	PLTH 1PE10.3,1X	TAUTOT 1PE10.3,1X
12	TAUTH 1PE10.3,1X	—	—	—	—	—	—

Notes: 1X: One blank space (ASCII code 32).
A10: 10 ASCII characters.
I10: Integer using up to 10 characters.
1PE10.3: Floating point number occupying at most 10 characters. Format: ±#.###E±##

Appendix E

Example of a 1-D file format

```
45950 TFTR 1 0 6        ;-SHOT #- F(X) DATA -UF1-DWR- 8-FEB-95
90/01/24                ;-SHOT DATE- UFILES ASCII FILE SYSTEM
 1                      ;-NUMBER OF ASSOCIATED SCALAR QUANTITIES-
2.0000E+00              ;-SCALAR, LABEL FOLLOWS:
RTCON:R_t cntrl
Time          seconds   ;-INDEPENDENT VARIABLE LABEL: X_
R_t (fit)     cm        ;-DEPENDENT VARIABLE LABEL-
2                       ;-PROC CODE- 0:RAW 1:AVG 2:SM. 3:AVG+SM
      86                ;-# OF PTS- X, F(X) DATA FOLLOW:

1.000000E-01  2.000000E-01  3.000000E-01  4.000000E-01  5.000000E-01  6.000000E-01
7.000000E-01  8.000000E-01  9.000000E-01  1.000000E+00  1.100000E+00  1.200000E+00
1.220000E+00  1.240000E+00  1.260000E+00  1.280000E+00  1.300000E+00  1.320000E+00
1.350000E+00  1.400000E+00  1.500000E+00  1.600000E+00  1.700000E+00  1.800000E+00
1.900000E+00  2.000000E+00  2.100000E+00  2.200000E+00  2.300000E+00  2.400000E+00
2.500000E+00  2.600000E+00  2.700000E+00  2.800000E+00  2.900000E+00  2.984600E+00
3.024600E+00  3.058600E+00  3.108600E+00  3.158600E+00  3.208600E+00  3.258600E+00
3.308600E+00  3.358600E+00  3.408600E+00  3.458600E+00  3.508600E+00  3.558600E+00
3.608600E+00  3.658600E+00  3.708600E+00  3.758600E+00  3.808600E+00  3.858600E+00
3.908600E+00  3.958600E+00  4.008600E+00  4.058600E+00  4.108600E+00  4.158600E+00
4.208600E+00  4.258600E+00  4.308600E+00  4.358600E+00  4.408600E+00  4.458600E+00
4.508600E+00  4.558600E+00  4.608600E+00  4.658600E+00  4.708600E+00  4.758600E+00
4.808600E+00  4.858600E+00  4.908600E+00  4.958600E+00  4.980400E+00  5.020400E+00
5.054400E+00  5.112200E+00  5.210500E+00  5.310500E+00  5.410500E+00  5.510500E+00
5.610500E+00  5.710500E+00
2.866400E+02  2.893800E+02  2.916400E+02  2.925800E+02  2.927900E+02  2.925300E+02
2.904900E+02  2.885700E+02  2.865100E+02  2.843400E+02  2.831500E+02  2.798400E+02
2.702600E+02  2.586100E+02  2.458400E+02  2.438500E+02  2.445000E+02  2.450100E+02
2.450300E+02  2.450800E+02  2.449700E+02  2.449600E+02  2.449200E+02  2.449500E+02
2.450400E+02  2.450400E+02  2.451700E+02  2.454800E+02  2.456500E+02  2.458400E+02
2.459200E+02  2.459300E+02  2.460200E+02  2.460900E+02  2.461600E+02  2.462200E+02
2.467500E+02  2.467700E+02  2.468700E+02  2.470600E+02  2.472200E+02  2.473900E+02
2.474700E+02  2.474900E+02  2.476000E+02  2.475600E+02  2.476500E+02  2.475900E+02
2.475800E+02  2.476100E+02  2.475600E+02  2.476200E+02  2.476100E+02  2.476000E+02
2.476000E+02  2.475300E+02  2.475900E+02  2.475900E+02  2.475900E+02  2.475900E+02
2.475800E+02  2.475500E+02  2.475700E+02  2.475800E+02  2.475700E+02  2.475500E+02
2.475800E+02  2.475900E+02  2.475400E+02  2.475600E+02  2.475300E+02  2.475800E+02
2.476000E+02  2.475500E+02  2.475900E+02  2.475500E+02  2.475400E+02  2.470800E+02
2.471400E+02  2.469700E+02  2.470200E+02  2.473500E+02  2.475100E+02  2.478200E+02
2.479400E+02  2.482700E+02

;------ END-OF-DATA ------------------ COMMENTS: ----------
```

Appendix F

Example of a 2-D file format

```
47379 T10 2          ;-SHOT #, TOK, DIMENSIONS
ASTRA                ;-SHOT DATE- UFILES ASCII FILE SYSTEM
0                    ;-NUMBER OF ASSOCIATED SCALAR QUANTITIES-
RHO                  ;-INDEPENDENT VARIABLE LABEL: X-
Time    seconds      ;-INDEPENDENT VARIABLE LABEL: Y-
TE                   ;-DEPENDENT VARIABLE LABEL-
0                    ;-PROC CODE-
      41             ;-# OF X PTS-
       2             ;-# OF Y PTS- X,Y,F(X,Y) DATA FOLLOW:


1.234568E-02  3.703704E-02  6.172840E-02  8.641975E-02  1.111111E-01  1.358025E-01
1.604938E-01  1.851852E-01  2.098766E-01  2.345679E-01  2.592593E-01  2.839506E-01
3.086420E-01  3.333333E-01  3.580247E-01  3.827161E-01  4.074074E-01  4.320987E-01
4.567901E-01  4.814815E-01  5.061728E-01  5.308642E-01  5.555556E-01  5.802469E-01
6.049383E-01  6.296296E-01  6.543210E-01  6.790124E-01  7.037037E-01  7.283951E-01
7.530864E-01  7.777778E-01  8.024692E-01  8.271605E-01  8.518519E-01  8.765432E-01
9.012346E-01  9.259260E-01  9.506173E-01  9.753087E-01  1.000000E+00
5.000000E-01  5.600000E-01
1.249955E+03  1.249928E+03  1.249857E+03  1.249699E+03  1.249357E+03  1.248623E+03
1.247049E+03  1.244089E+03  1.240349E+03  1.235955E+03  1.230638E+03  1.223565E+03
1.213359E+03  1.201025E+03  1.186267E+03  1.168705E+03  1.147269E+03  1.118974E+03
1.085838E+03  1.046929E+03  1.002762E+03  9.553096E+02  9.045463E+02  8.507968E+02
7.926033E+02  7.301635E+02  6.663555E+02  6.032237E+02  5.410034E+02  4.802980E+02
4.216935E+02  3.655893E+02  3.139088E+02  2.650629E+02  2.181746E+02  1.735605E+02
1.329235E+02  1.003913E+02  7.351675E+01  5.036697E+01  3.000000E+01  3.238552E+03
3.235825E+03  3.231117E+03  3.223967E+03  3.212425E+03  3.196941E+03  3.177711E+03
3.153886E+03  3.127802E+03  3.100414E+03  3.070344E+03  3.033709E+03  2.984734E+03
2.927280E+03  2.860039E+03  2.784092E+03  2.701305E+03  2.609718E+03  2.508890E+03
2.392746E+03  2.262020E+03  2.123718E+03  1.980231E+03  1.833160E+03  1.681956E+03
1.527917E+03  1.375882E+03  1.231912E+03  1.093661E+03  9.611416E+02  8.350384E+02
7.155447E+02  6.068830E+02  5.053905E+02  4.094046E+02  3.198300E+02  2.398611E+02
1.785490E+02  1.292567E+02  8.577742E+01  4.500000E+01

;---- END-OF-DATA ----------COMMENTS: ----------
**************************************
**************************************
```

Acknowledgements

Part of this work is jointly funded by UK DTI, Euratom and USDOE.

References

[1] Yushmanov, P., et al., Nucl. Fusion **30** (1990) 1999.
[2] Christiansen, J.P., et al., Nucl. Fusion **32** (1992) 291.
[3] Ryter, F., et al., Nucl. Fusion **36** (1992) 1217.
[4] Kotschenreuther, M., Dorland W., Beer M.A., Hammett G.W., Phys. Plasmas **2** (1995) 2381.
[5] Waltz, R.E., et al., Phys. Plasmas **4** (1997) 2482.
[6] Kinsey, J., Bateman, G., Phys. Plasmas **3** (1996) 3344.
[7] Itoh, K., Itoh, S.-I., Fukuyama, A., Azumi, M., Plasma Phys. Control. Fusion **36** (1994) 279.
[8] Boucher, D., Rebut, P.-H., in Advances in Simulations of Modelling of Thermonuclear Plasmas (Proc. Tech. Comm. Mtg Montreal, 1992), IAEA, Vienna (1993) 142.
[9] Vlad, G., et al., Nucl. Fusion **38** (1998) 557.
[10] Dnestrovskij, Yu.N., Lysenko, S.E., Tarasyan, K.N., Nucl. Fusion **35** (1995) 1047.
[11] Connor, J.W., et al., in Fusion Energy 1996 (Proc. 16th Int. Conf. Montreal, 1996), Vol. 2, IAEA, Vienna (1997) 935.
[12] Mikkelsen, D., et al., in Fusion Energy 1998 (Proc. 17th Int. Conf. Yokohama, 1998), CD-ROM, IAEA, Vienna (1999) paper ITERP1/08.
[13] ITER Physics Expert Groups on Confinement and Transport and Confinement Modelling and Databases, ITER Physics Basis Editors, Nucl. Fusion **39** (1999) 2175.
[14] Neuhauser, J., et al., Plasma Phys. Control. Fusion **37** (1995) A37.
[15] Hutchinson, I., et al., Phys. Plasmas **1** (1994) 1511.
[16] Greenwald, M., et al., Phys. Plasmas **2** (1995) 2308.
[17] Greenwald, M., et al., Nucl. Fusion **37** (1997) 793.
[18] Rice, J., et al., Nucl. Fusion **38** (1998) 75.
[19] Luxon, J.L., et al., in Plasma Physics and Controlled Nuclear Fusion Research 1986 (Proc. 11th Int. Conf. Kyoto, 1986), Vol. 1, IAEA, Vienna (1987) 159.
[20] Waltz, R.E., et al., Phys. Rev. Lett. **65** (1990) 2390.
[21] Waltz, R.E., et al., Nucl. Fusion **32** (1992) 1051.
[22] DeBoo, J.C., et al., in Controlled Fusion and Plasma Physics (Proc. 18th Eur. Conf. Berlin, 1991), Vol. 15C, Part I, European Physical Society, Geneva (1991) 173.
[23] Petty, C.C., et al., Phys. Rev. Lett. **74** (1995) 1763.
[24] Petty, C.C., et al., Phys Plasmas **2** (1995) 2343.
[25] Petty, C.C., et al., Nucl. Fusion **38** (1998) 1183.
[26] Schissel, D., et al., Nucl. Fusion **34** (1994) 1401.
[27] Schissel, D., et al., Plasma Phys. Control. Fusion **38** (1996) 1487.
[28] Greenfeld, C.M., et al., Nucl. Fusion **37** (1997) 1215.
[29] Schissel, D., et al., in Fusion Energy 1996 (Proc. 16th Int. Conf. Montreal, 1996), Vol. 1, IAEA, Vienna (1997) 463.
[30] Rice, B., et al., Nucl. Fusion **36** (1996) 1271.
[31] Andreani, R., et al., in Fusion Technology (Proc. 16th Symp. London, 1990), Vol. 1, North-Holland, Amsterdam (1991) 2118.
[32] Buratti, P., et al., Phys. Rev. Lett. **82** (1999) 560.
[33] Keilhacker, M., et al., Nucl. Fusion **39** (1999) 209.
[34] Balet, B., Cordey, J.G., Stubberfield, P.M., Plasma Phys. Control. Fusion **34** (1992) 3.
[35] JET Team, Nucl. Fusion **32** (1992) 187.
[36] Balet, B., et al., Nucl. Fusion **33** (1993) 1345.
[37] Balet, B., et al., in Controlled Fusion and Plasma Physics (Proc 22nd Eur. Conf. Bournemouth, 1995), Vol. 19C, Part I, European Physical Society, Geneva (1995) 9.
[38] Cordey, J.G., et al., in Controlled Fusion and Plasma Physics (Proc. 24th Eur. Conf. Berchtesgaden, 1997), Vol. 21A, Part III, European Physical Society, Geneva (1997) 1045.
[39] Matthews, G.F., et al., ibid., p. 1045.
[40] Soldner, F.X., et al., Nucl. Fusion **39** (1999) 407.
[41] Soldner, F.X., JET Team, Plasma Phys. Control. Fusion **39** (1997) B353.
[42] Parail, V., et al., Nucl. Fusion **39** (1999) 429.
[43] Gormezano, C., JET Team, in Fusion Energy 1996 (Proc. 16th Int. Conf. Montreal, 1996), Vol. 1, IAEA, Vienna (1997) 487.
[44] Tobita, K., JT-60 Team, Plasma Phys. Control. Fusion **41** (1999) A333.
[45] Ishida, S., JT-60 Team, Nucl. Fusion **39** (1999) 1211.
[46] Kusama, Y., JT-60 Team, Phys. Plasmas **6** (1999) 1935.
[47] Shirai, H., et al., J. Phys. Soc. Jpn. **64** (1995) 4209.
[48] Shirai, H., et al., Plasma Phys. Control. Fusion **38** (1996) 1455.
[49] Shirai, H., et al., Nucl. Fusion **39** (1999) 1713.
[50] Shirai, H., JT-60 Team, Phys. Plasmas **5** (1998) 1712.
[51] Lopes Cardozo, N.J., et al., in Fusion Energy 1998 (Proc 17th Int. Conf. Yokahama, 1998), CD-ROM, IAEA, Vienna (1999) paper EX7/4.
[52] Hogeweij, G.M.D., et al., Phys. Rev. Lett. **76** (1996) 632.
[53] Lopes Cardozo, N.J., et al., Plasma Phys. Control. Fusion **39** (1997) B303.
[54] Esipchuk, Yu.V., Kislov, A.Ya., Semashko, A.N., Tarasyan, K.N., J. Moscow Phys. Soc. **1** (1991) 119.
[55] Hawryluk, R.J., et al., Phys. Plasmas **5** (1998) 1577.
[56] Hawryluk, R.J., et al., Phil. Trans. R. Soc. Lond. A **357** (1999) 443.

[57] Phillips, C.K., et al., Phys. Rev. Lett. **79** (1997) 1050.
[58] Efthimion, P.C., et al., Phys. Rev. Lett. **66** (1991) 421.
[59] Zarnstorff, M., et al., in Plasma Physics and Controlled Nuclear Fusion Research 1990 (Proc. 13th Int. Conf. Washington, DC, 1990), Vol. 1, IAEA, Vienna (1991) 109.
[60] Zarnstorff, M., et al., in Plasma Physics and Controlled Nuclear Fusion Research 1992 (Proc. 14th Int. Conf. Würzburg, 1992), Vol. 1, IAEA, Vienna (1993) 111.
[61] Perkins, F.W., et al., Phys. Fluids B **5** (1993) 477.
[62] Batha, S., et al., in Controlled Fusion and Plasma Physics (Proc. 24th Eur. Conf. Berchtesgaden, 1997), Vol. 21A, Part III, European Physical Society, Geneva (1997) 1057.
[63] Scott, S.D., et al., in Fusion Energy 1996 (Proc. 16th Int. Conf. Montreal, 1996), Vol. 1, IAEA, Vienna (1997) 573.
[64] Budny, R.V., et al., Nucl. Fusion **34** (1994) 1247.
[65] Strachan, J.D., et al., Phys. Rev. Lett. **72** (1994) 3526.
[66] Budny, R.V., et al., Nucl. Fusion **35** (1995) 1497.
[67] Zarnstorff, M., et al., in Plasma Physics and Controlled Nuclear Fusion Research (Proc. 15th Int. Conf. Seville, 1994), Vol. 1, IAEA, Vienna (1995) 183.
[68] Scott, S.D., et al., Phys. Plasmas **2** (1995) 2299.
[69] Scott, S.D., et al., Phys. Scr. **51** (1995) 394.
[70] McKee, et al., Phys. Rev. Lett. **75** (1995) 649.
[71] Sabbagh, S.A., et al., in Fusion Energy 1996 (Proc. 16th Int. Conf. Montreal, 1996), Vol. 1, IAEA, Vienna (1997) 921.
[72] Hill, K.W., et al., Phys. Plasmas **6** (1999) 877.
[73] Bush, C.E., et al., Phys. Plasmas **2** (1995) 2366.
[74] Bush, C.E. et al., Plasma Phys. Control. Fusion **38** (1996) 1353.
[75] Levinton, F.M. et al., Phys. Rev. Lett. **75** (1995) 4417.
[76] Synakowski, E.J., et al., Phys. Rev. Lett. **78** (1997) 2972.
[77] Ramsey, A.T., Nucl. Fusion **31** (1991) 1811.
[78] Scott, S.D., et al., in 1992 International Conference on Plasma Physics (Proc. Conf. Innsbruck, 1992), Vol. 16C, Part I, European Physical Society, Geneva (1992) 39.
[79] Kissick, M., et al., Nucl. Fusion **36** (1996) 1691.
[80] Kissick, M., et al., Nucl. Fusion **37** (1997) 568.
[81] Equipe Tore Supra (presented by R. Aymar) in Plasma Physics and Controlled Nuclear Fusion Research 1988 (Proc. 12th Int. Conf. Nice, 1988), Vol. 1, IAEA, Vienna (1989) 9.
[82] Hoang, G.T., et al., Nucl. Fusion **34** (1994) 75.
[83] Equipe Tore Supra, Plasma Phys. Control. Fusion **38** (1996) A251.
[84] Hoang, G.T., et al., Nucl. Fusion **38** (1998) 117.
[85] Messiaen, A., et al., Phys Plasmas **4** (1997) 1690.
[86] Ongena, J., et al., Nucl. Fusion **33** (1993) 283.
[87] Kinsey, J.E., et al., Phys. Plasmas **6** (1999) 1865.
[88] Sugihara, M., et al., in Controlled Fusion and Plasma Physics (Proc 26th Eur. Conf. Maastricht, 1999), Vol. 23J, European Physical Society, Geneva (1999) 1449.
[89] Biglari, H., Diamond, P.H., Terry, P.W., Phys Fluids B **2** (1990) 1.
[90] Houlberg, W.A., Shaing, K.C., Hirshman, S.P., Zarnstorff, M.C., Phys Plasmas **4** (1997) 3230.
[91] Lao, L.L., St John, H., Stambaugh, R.D., Kellman A.G., Pfeiffer, W., Nucl Fusion **25** (1985) 1611.

(Manuscript received 13 March 2000
Final manuscript accepted 1 August 2000)

E-mail address of J.W. Connor:
jack.connor@ukaea.org.uk

Subject classification: F2, Tm